

Synthesis, Structural Characterization, and Electronic Structure of Single-Crystalline $\text{Cu}_x\text{V}_2\text{O}_5$ Nanowires

Christopher J. Patridge,[†] Chernoy Jaye,[‡] Hengsong Zhang,[†] Amy C. Marschilok,[§] Daniel A. Fischer,[‡] Esther S. Takeuchi,^{†,§,||} and Sarbajit Banerjee^{*,†}

Department of Chemistry, Department of Electrical Engineering, and Department of Chemical and Biological Engineering, University at Buffalo, State University of New York, Buffalo, New York 14260-3000, and Materials Science and Engineering Laboratory, National Institute of Standards and Technology, Gaithersburg, Maryland 20899

Received December 17, 2008

Single-crystalline copper vanadium oxide nanowires β' - $\text{Cu}_x\text{V}_2\text{O}_5$ ($x \sim 0.60$) have been synthesized by the hydrothermal reduction of bulk CuV_2O_6 using small-molecule aliphatic alcohols as reducing agents. The prepared copper vanadium bronze nanowires are metallic in nature and exhibit aspect ratios as high as 300. The recent discovery of superconductivity and charge disproportionation in bulk β' - $\text{Cu}_x\text{V}_2\text{O}_5$ has led to renewed interest in these one-dimensional metallic systems. Scaling these systems to nanoscale dimensions offers the potential for further tunability of electronic transport and Li-ion intercalation kinetics. A combination of spectroscopic and electrical measurement methods has been used to provide evidence for the metallic nature and the presence of room-temperature charge disproportionation in these nanowires.

Introduction

The incorporation of monovalent and divalent metals into the layered framework of vanadium pentoxide has been studied extensively over the last fifty years. The wide range of available oxidation states of vanadium provides a myriad of compounds and coordination modes. Of the different stoichiometric vanadium oxides, the tunnel-like framework of V_2O_5 is especially notable since it allows the facile intercalation of a variety of organic and inorganic guest species.^{1,2} A rich diversity of vanadium bronzes and intercalation compounds based on the incorporation of either alkali or transition metals within the interstitial spaces of the V_2O_5 tunnel framework have been extensively studied in recent years. Vanadium bronzes show very remarkable transport and magnetic properties some of which have only recently been discovered including metal–insulator transi-

tions,³ charge and spin ordering,⁴ paramagnetism,⁵ gapless states, and superconductivity.⁵ The facile variations in stoichiometry that can be achieved in these systems^{6–10} point to the possibility of finely tuning electron transport in these materials. Wadsley et al.¹¹ reported the first vanadium bronzes incorporating Na^+ ions with the stoichiometry $\text{Na}_x\text{V}_2\text{O}_5$ and showed that the addition of metal cations does not significantly alter the structure and size of the V_2O_5 framework. The V_2O_5 tunnel framework is composed of three crystallographically distinct vanadium sites. The first set of vanadium atoms (V1) lie at the centers of VO_6 octahedra

* To whom correspondence should be addressed. E-mail: sb244@buffalo.edu.

[†] Department of Chemistry, State University of New York, Buffalo.

[‡] National Institute of Standards and Technology.

[§] Department of Electrical Engineering, State University of New York, Buffalo.

^{||} Department of Chemical and Biological Engineering, State University of New York, Buffalo.

(1) Livage, J. *Chem. Mater.* **1991**, 3 (4), 578–593.

(2) Wang, Y.; Cao, G. Z. *Chem. Mater.* **2006**, 18 (12), 2787–2804.

(3) Villeneuve, G.; Kessler, H.; Chaminade, J. P. *J. Phys., Colloq.* **1976**, (4), 79–82.

(4) Yamaura, J.; Yamauchi, T.; Ninomiya, E.; Sawa, H.; Isobe, M.; Yamada, H.; Ueda, Y. *J. Magn. Magn. Mater.* **2004**, 272–276 (1), 438–439.

(5) Ueda, Y.; Isobe, M.; Yamauchi, T. *J. Phys. Chem. Solids* **2002**, 63 (6–8), 951–955.

(6) Gopalakrishnan, R.; Chowdari, B. V. R.; Tan, K. L. *Solid State Ionics* **1992**, 53–56 (2), 1168–71.

(7) Kato, K.; Takayama-Muromachi, E.; Kanke, Y. *Acta Crystallogr., Sec. C* **1989**, C45 (12), 1845–1847.

(8) Kato, K.; Takayama-Muromachi, E.; Kanke, Y. *Acta Crystallogr., Sec. C* **1989**, C45 (12), 1841–1844.

(9) Nagao, N.; Nogami, Y.; Oshima, K.; Yamada, H.; Ueda, Y. *Phys. B: Cond. Mat.* **2003**, 329–333 (2), 713–714.

(10) Pereira-Ramos, J. P.; Messina, R.; Znaidi, L.; Baffier, N. *Solid State Ionics* **1988**, 28–30 (1), 886–894.

(11) Wadsley, A. D. *Acta Crystallogr.* **1955**, 8, 695–701.

that share edges to form double chains; the second set of vanadium atoms (V2) lie at the centers of VO₆ octahedra that form two-legged ladder-like layers by sharing corners; the third set of vanadium (V3) sites are within VO₅ square pyramids that share edges to form double chains. The zigzag double-chain and ladder-like framework formed by the VO₆ and VO₅ polyhedra along the *b*-axis constitute a tunnel structure that is able to accommodate cations at specific sites. Two distinct classes of M_xV₂O₅ bronzes are known (β and β') that essentially retain the V₂O₅ tunnel framework and differ only in the sites occupied by the metal cations. Most cations upon incorporation into the V₂O₅ framework yield β -M_xV₂O₅ bronzes wherein they occupy a 5-coordinated site within the tunnels; in the β -phase the chains of cations are separated by 2.2–2.3 Å, and owing to this small separation, nearest neighbor sites in the *ac* plane can not be simultaneously occupied, yielding a theoretical maximum value of $x = 0.33$.¹² In contrast, Li⁺ and Cu⁺ yield β' -M_xV₂O₅ bronzes wherein metal ions occupy tetrahedral MO₄ and trigonally coordinated MO₃ sites that are shifted by half a unit cell length from the sites occupied in the β phase. The separation between chains of cations that are thus coordinated is significantly larger than for the β phase, approaching close to 3.7 Å.¹² The smaller size and greater separation between cations allows the incorporation of significantly greater amounts of Cu ranging up to a theoretical maximum of $x = 0.67$.¹³ In a series of articles, the groups of Ueda, Yamaura, and Yamada have painstakingly mapped out the phase diagram of Cu_xV₂O₅ as a function of temperature, pressure, and Cu concentration.^{5,9,12,14} The ground-state of the β' phase is characterized by metallic behavior for $x > 0.40$. Indeed, the conductivity of the β' -copper vanadium bronzes shows a significantly decreased transport barrier as the Cu content increases to ~ 0.60 .¹² However, unlike β -M_xV₂O₅ phases that show discontinuous insulator–metal phase transitions with the increasing incorporation of metal ions, the Cu_xV₂O₅ β' -phases tend to show a smooth increase in conductivity with increasing copper concentration. The conductivity of both β and β' phases arises from the reduction of V⁵⁺ framework ions to V⁴⁺ followed by one-dimensional (1D) charge ordering along the framework. Several possible charge ordering patterns have been proposed to explain conduction through the tunnel framework including a linear chain or rectangular charge ordering pattern on the V2–V2 ladder for various β -M_{0.33}V₂O₅ bronzes and a straight-chain charge disproportionation motif accompanied by structural deformation on the V2–V2 ladder for β' -Cu_{0.65}V₂O₅.^{15a} Indeed, superconductivity has been observed at around 3 GPa pressure and 6 K for the β' -Cu_{0.65}V₂O₅ phase.⁵ The crystal structure of the superconducting phase is characterized as a quasi 1D system at high pressure because of the large

anisotropy between excellent conduction along the *b*-axis and poor conduction along the *a* and *c* axes. Indeed, Ma et al. have proposed that the superconductivity observed at high pressures originates from charge transfer from partially occupied V1–V3 chains to V2–V2 ladders.^{15a} The availability of highly anisotropic 1D nanowires with lateral dimensions smaller than the coherence length will allow the investigation of quantum phase slip properties that give rise to finite resistance below T_c in these novel superconductors.^{15b} The Mermin–Wagner theorem states that long-range superconducting order can not exist in a truly 1D system; the fabrication of single-crystalline vanadium bronze nanowires will enable evaluation of the role of thermal and quantum phase slips in broadening and extinguishing superconductivity in these materials. The extent of copper doping also strongly influences the magnetic susceptibility,^{15a} structural charge ordering,^{12,4} and bipolaron formation^{16,17} in Cu_xV₂O₅.¹⁸

More recently, the high conductivity and increased interlayer separation in copper vanadium bronzes has led to their exploration as high-capacity cathode materials for Li-ion batteries.^{19–23} Scaling copper vanadium bronzes to nanoscale dimensions offers the opportunity to further tune electronic transport, magnetic properties, and the Li-ion storage capacities and intercalation kinetics of these systems. In terms of their use as cathode materials, nanostructured copper vanadium bronzes may potentially show improved power and energy densities because of improved solid-state diffusion kinetics, better interfacial contact with the electrolyte, and the operation of Li-ion storage mechanisms not accessible for bulk materials.²⁴ Recently, Cui and co-workers have demonstrated the completely reversible lithiation and delithiation of high-aspect-ratio sub-100 nm diameter V₂O₅ nanowires even for lithiated phases Li_xV₂O₅ with x approaching 3.0.²⁵ In contrast, in bulk V₂O₅ the lithiation process (and the formation of the lithium vanadium bronze) is irreversible at such stoichiometries. The greater conductivity of the Cu_xV₂O₅ nanowires compared to V₂O₅ (an *n*-type semiconductor) is likely to lead to improved Li-ion insertion/extraction kinetics and better cycling behavior. A longstanding objective in the electrochemistry community has been the fabrication of novel battery architectures based on arrays of nanowires/nanorods vertically aligned on collector electrodes such that the charging/discharging of individual

- (12) Yamada, H.; Ueda, Y. *J. Phys. Soc. Jpn.* **2000**, *69* (5), 1437–1442.
 (13) Streltsov, V. A.; Nakashima, P. N. H.; Sobolev, A. N.; Ozerov, R. P. *Acta Crystallogr., Sec. B* **2005**, *B61* (1), 17–24.
 (14) Yamaura, J.-I.; Yamauchi, T.; Isobe, M.; Yamada, H.; Ueda, Y. *J. Phys. Soc. Jpn.* **2004**, *73* (4), 914–920.
 (15) (a) Ma, C.; Yang, H. X.; Li, Z. A.; Ueda, Y.; Li, J. Q. *Solid State Commun.* **2008**, *146* (1–2), 30–34. (b) Lau, C. N.; Markovic, N.; Bockrath, M.; Bezryadin, A.; Tinkham, M. *Phys. Rev. Lett.* **2001**, *87*, 217003/1–217003/4.

- (16) Chakraverty, B. K.; Sienko, M. J.; Bonnerot, J. *Phys. Rev. B* **1978**, *17* (10), 3781.
 (17) Nagasawa, H.; Onoda, M.; Kanai, Y.; Kagoshima, S. *Synth. Met.* **1987**, *19* (1–3), 971–976.
 (18) Nithya, R.; Chandra, S.; Reddy, G. L. N.; Sahu, H. K.; Sastry, V. S. *Los Alamos Natl. Lab. Cond. Mater.* **2004**, 1–9.
 (19) Andrukaitis, E. *J. Power Sources* **1997**, *68* (2), 652–655.
 (20) Andrukaitis, E.; Cooper, J. P.; Smit, J. H. *J. Power Sources* **1995**, *54* (2), 465–469.
 (21) Li, H. X.; Jiao, L. F.; Yuan, H. T.; Zhao, M.; Zhang, M.; Wang, Y. M. *Mater. Lett.* **2007**, *61* (1), 101–104.
 (22) Souza, E. A.; Lourenco, A.; Gorenstein, A. *Solid State Ionics* **2007**, *178* (5–6), 381–385.
 (23) Wei, Y.; Ryu, C.-W.; Kim, K.-B. *J. Power Sources* **2007**, *165* (1), 386–392.
 (24) Arico, A. S.; Bruce, P.; Scrosati, B.; Tarascon, J.-M.; van Schalkwijk, W. *Nat. Mater.* **2005**, *4* (5), 366–377.
 (25) Chan, C. K.; Peng, H.; Twisten, R. D.; Jarausch, K.; Zhang, X. F.; Cui, Y. *Nano Letters* **2007**, *7* (2), 490–495.

nanowires controls the power rate of the battery. The highly anisotropic $\text{Cu}_x\text{V}_2\text{O}_5$ nanowires prepared here are likely to be excellent building blocks for such cathode geometries. The small lateral dimensions of these nanowires are conducive to rapid Li-ion insertion, extraction, and diffusion, whereas the long lengths will provide high storage capacities.

In this Article, we report the first synthesis of single-crystalline metallic copper vanadate nanowires with aspect ratios exceeding 300. The availability of these novel 1D nanostructures will provide new insight into the effect of finite size on electron transport and Li-ion intercalation in copper vanadium bronzes. A previous report in the literature points to the fabrication of CuV_2O_6 nanowires via the hydrothermal reaction of aqueous NH_4VO_3 and CuCl_2 .²⁶ However, the absence of V^{4+} makes this system less interesting from both solid-state physics and electrochemical perspectives since the primary conduction path is thought to be along V^{4+} ladders. Furthermore, the α - CuV_2O_6 nanowires synthesized via the hydrothermal approach are polycrystalline with a very high density of grain boundaries. Slightly oxygen-deficient hydrated $\text{M}_x\text{V}_2\text{O}_5 \cdot x\text{H}_2\text{O}$ nanowires have also been previously reported in the literature but the hydrated structure shows significant differences from that of vanadium bronzes.²⁷ Furthermore, Liu et al. have reported the fabrication of single-crystalline $\text{Ag}_{0.33}\text{V}_2\text{O}_5$ nanowires by the hydrothermal reaction of aqueous AgNO_3 with NH_4VO_3 .²⁸ Most notably, Balkus and co-workers have reported the clean synthesis of ultralong orthorhombic V_2O_5 nanowires and have also extended this synthesis to the preparation of silver vanadium oxide structures.²⁹ Here, we use the hydrothermal reduction of a solid-state CuV_2O_6 precursor by small-molecule aliphatic alcohols to form single-crystalline $\text{Cu}_{0.60}\text{V}_2\text{O}_5$ nanowires with high aspect ratios.

Experimental Section

Synthesis. Bulk CuV_2O_6 powder was synthesized by mixing CuO powder (Sigma-Aldrich >99%) and V_2O_5 powder (Sigma-Aldrich 99.5%) in 1:1 molar ratio.^{30,31} The mixture was heated in a muffle furnace at 620 °C for 48 h and then allowed to cool to room temperature. Next, 300 mg of the prepared CuV_2O_6 product was placed in a Teflon cup and heated in a sealed autoclave (Parr) along with 0.1–4.0 mL of 2-propanol mixed with deionized water to bring the total liquid volume to 16 mL. The hydrothermal reaction was performed for 3–7 days at 210 °C. Upon cooling to room temperature, the solid product was vacuum-filtered, washed repeatedly with deionized water and ethanol, and dried at 110 °C for 24 h. In analogous reactions, 2-propanol was substituted with methanol, ethanol, and octanol.

Characterization. Powder X-ray diffraction (XRD) data was collected in Bragg–Brentano geometry using a Rigaku Ultima IV

instrument (Cu $\text{K}\alpha$ radiation, voltage 40 kV, current 44 mA). The samples were ground to a fine powder and packed in a sample holder with 0.5 mm depth for the powder XRD measurements. Pattern fitting and phase identification were achieved with the help of JADE 8.5. The morphology of the hydrothermally prepared product was evaluated by scanning electron microscopy (Hitachi S4000 cold field emission at 25 kV), transmission electron microscopy (JEOL-100-CX-II at 100 kV operating voltage), and by combining high-resolution transmission electron microscopy (HRTEM) with selected area electron diffraction (SAED, JEOL-2010, 200 kV, 100 μA). For electron microscopy observations, the samples were dispersed in 2-propanol using a bath sonicator and then deposited onto 300 mesh carbon-coated Cu grids. High-resolution X-ray photoelectron spectroscopy (XPS) data was obtained using a Perkin-Elmer PHI 660 instrument. Four-point probe electrical measurements of $\text{Cu}_x\text{V}_2\text{O}_5$ nanowire pellets were made using a home-built apparatus based on a Keithley-220 current source and a Keithley-6517 power supply. Fourier transform infrared (FTIR) data was obtained on a Nicolet Magna 550 instrument in transmission mode for pellets prepared by mixing the samples with KBr. Near-edge X-ray absorption fine structure (NEXAFS) spectroscopy data was collected on National Institute of Standards and Technology beamline U7A at the National Synchrotron Light Source of Brookhaven National Laboratory with a toroidal mirror spherical grating monochromator using a 1200 lines/mm grating and an energy resolution of 0.1 eV. NEXAFS spectra were collected in partial electron yield (PEY) mode with a channeltron multiplier near the sample surface using the detector at -200 V bias to enhance surface sensitivity. The PEY signal was normalized by the drain current of a clean gold mesh located along the path of the incident X-rays. In addition, all the data was collected in conjunction with a standard V reference mesh for energy calibration.

Results and Discussion

The bulk CuV_2O_6 precursor prepared by the high-temperature solid-state reaction has been characterized by XRD. The XRD reflections can be indexed to a triclinic phase of CuV_2O_6 (Joint Committee on Powder Diffraction Standards (JCDPS) 00-045-1054, $a = 9.172$ Å, $b = 3.546$ Å, $c = 6.482$ Å; $\alpha = 92.3$, $\beta = 110.32$, $\gamma = 91.85$). After hydrothermal reduction with aliphatic alcohols, XRD data indicates that CuV_2O_6 is converted to $\text{Cu}_x\text{V}_2\text{O}_5$ with x estimated to be 0.55–0.65. The product diffraction pattern can be indexed to a monoclinic phase of $\text{Cu}_{(0.55 - 0.65)}\text{V}_2\text{O}_5$ (JCDPS 79-007-7609) with $a = 15.2007$ Å, $b = 3.6725$ Å, $c = 10.0927$ Å, $\beta = 106.31$ ^{18,32,33} along with some other minor phases as discussed below. Figure 1 shows the indexed XRD patterns for the product obtained by the hydrothermal reduction of the precursor with 2 mL of 2-propanol for 7 days. The normalized theoretical intensities match very well with the experimental diffraction pattern. A visualization of the crystal structure depicting the $\text{Cu}_x\text{V}_2\text{O}_5$ unit cell is shown in Figure 2. As noted above, two distinct locations inside the V_2O_5 framework are partially occupied by Cu^+ ions. The Cu^+ ions are located on the mirror plane of $4i$ (tetrahedrally coordinated by four oxygen atoms) and on the $8j$ position

(26) Ma, H.; Zhang, S.; Ji, W.; Tao, Z.; Chen, J. *J. Am. Chem. Soc.* **2008**, *130* (15), 5361–5367.

(27) Melghit, K.; Al-belushi, M. *Mater. Lett.* **2008**, *62* (19), 3358–3360.

(28) Liu, Y.; Zhang, Y.; Zhang, M.; Qian, Y. *J. Cryst. Growth* **2006**, *289* (1), 197–201.

(29) Xiong, C. R.; Aliev, A. E.; Gnade, B.; Balkus, K. J. *ACS Nano* **2008**, *2* (2), 293–301.

(30) Prokofiev, A. V.; Kremer, R. K.; Assmus, W. *J. Cryst. Growth* **2001**, *231* (4), 498–505.

(31) Sakurai, Y.; Ohtsuka, H.; Yamaki, J.-i. *J. Electrochem. Soc.* **1988**, *135* (1), 32–36.

(32) Galy, J.; Lavaud, D.; Casalat, A.; Hagenmuller, P. *J. Solid State Chem.* **1970**, *2* (4), 531–543.

(33) Savariault, J. M.; Deramond, E.; Galy, J. *Z. Kristallogr.* **1994**, *209* (5), 405–412.

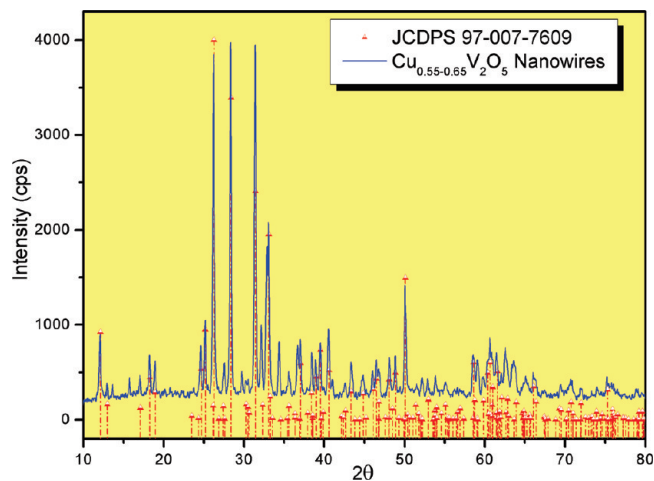


Figure 1. XRD pattern of $\text{Cu}_x\text{V}_2\text{O}_5$ nanowires prepared by the hydrothermal reduction of CuV_2O_6 by 2-propanol for 7 days shown alongside the PDF pattern 97-007-7609 corresponding to the diffraction pattern of $\text{Cu}_{0.59}\text{V}_2\text{O}_5$.

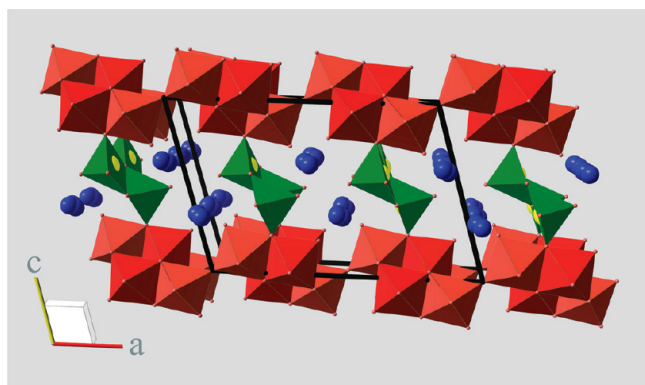


Figure 2. Crystal Structure of $\text{Cu}_{0.55-0.65}\text{V}_2\text{O}_5$. Cu (blue) atoms reside at two positions within the V_2O_5 framework (red VO_6 and green VO_5). The unit cell is visible near the middle of the image looking down the b -axis.

(trigonally coordinated by three oxygen atoms). In this structure, two crystallographically distinct vanadium atoms, V1 and V2, form double VO_6 octahedra with edge sharing along the b -direction. The third distinct, vanadium site, V3, connects the double octahedra along the c -direction and has an edge-sharing square pyramidal local geometry. Because of variable copper content, convergent beam electron diffraction at low temperature has been used to establish the $C2/m$ space group assignment for these β' vanadium bronzes.¹³ Figures 1 and 3 show noticeable differences in the relative intensities of reflections for samples prepared by hydrothermal reduction with different alcohols for varying times. These changes can be attributed to the strongly preferred orientation present in the 1D nanowire products that is somewhat retained even after mechanical grinding of the samples (which does not appear to break the nanowires).

Figure 3 compares the XRD pattern of the CuV_2O_6 starting material to the products obtained after hydrothermal reduction with varying amounts of 2-propanol. A very low intensity peak at 29.6° which matches well with the strongest reflection of the precursor CuV_2O_6 phase is seen for all the products evidencing the persistence of some of the starting material. Most notably, the presence of a hydrated volborthite

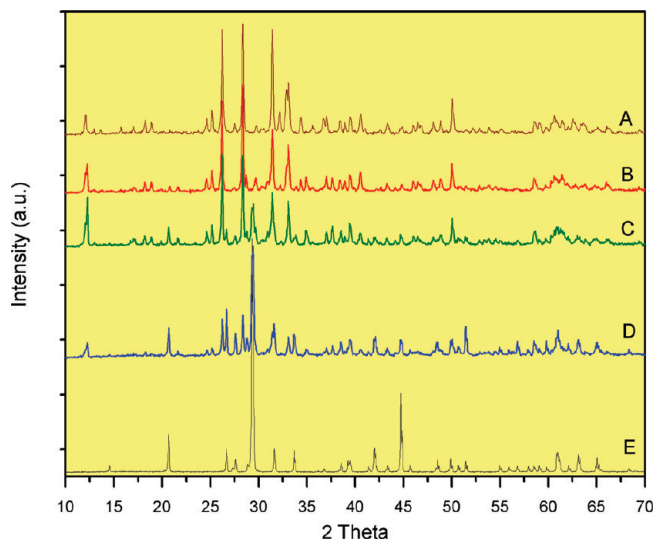
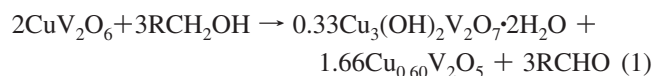


Figure 3. XRD patterns of $\text{Cu}_x\text{V}_2\text{O}_5$ nanowires prepared by the reduction of micrometer-size bulk CuV_2O_6 by (A) 2 mL, (B) 500 μL , (C) 250 μL , (D) 100 μL of 2-propanol. (E) XRD pattern of micrometer-sized CuV_2O_6 .

phase with the nominal stoichiometry $\text{Cu}_3(\text{OH})_2\text{V}_2\text{O}_7 \cdot 2\text{H}_2\text{O}$ (97-007-3282) is noted and the relative concentration of this phase appears to be significantly greater when the 2-propanol content is decreased in the reaction mixture. This hydrated phase has been proposed as an intermediate to the formation of CuV_2O_6 nanowires by a hydration, exfoliation, splitting process and is a naturally occurring mineral found in oxidized zones of vanadium-containing hydrothermal deposits.³⁴ The degree of hydration appears to vary somewhat across different experimental runs as indicated by DSC measurements. However, XRD measurements indicate the retention of the basic volborthite framework. As discussed in more detail below, this phase is likely a byproduct of the disproportionation reaction that yields $\text{Cu}_x\text{V}_2\text{O}_5$ nanowires. Most notably, these copper vanadium bronze nanowires are not formed when CuV_2O_6 is treated hydrothermally with DI water without the addition of any alcohols.

Upon hydrothermal treatment in the presence of alcohols, a disproportionation reaction is thought to yield the Cu-rich volborthite phase and the copper-deficient $\text{Cu}_x\text{V}_2\text{O}_5$ phase as per



Notably, some deviation from the above stoichiometries is likely, especially with regards to the extent of hydration and hydroxylation of the volborthite phase but is difficult to monitor because of the low concentrations of this phase. The stoichiometry of this reaction implies the predominance of the copper-deficient vanadium bronze phase, as is indeed experimentally observed. However, the relative proportion of the $\text{Cu}_{0.60}\text{V}_2\text{O}_5$ nanowires in the product seems to be in excess of the amounts expected from eq 1. This can be attributed to the hydrothermal decomposition of the volbor-

(34) Zhang, S.; Li, W.; Li, C.; Chen, J. *J. Phys. Chem. B* **2006**, *110* (49), 24855–24863.

thite phase into CuV_2O_6 and CuO as reported previously in the literature.²⁶



This reaction yields CuV_2O_6 , which is then further transformed to the copper vanadium bronze nanowires according to eq 1. XPS measurements indicate the presence of some Cu(II) species corresponding to trace CuO present in the samples; some soluble copper species are also likely lost during the filtration of the nanowire product.

At low alcohol concentrations (100–500 μL), the transformation of CuV_2O_6 to $\text{Cu}_x\text{V}_2\text{O}_5$ is incomplete even after reaction for 7 days. The $\text{Cu}_x\text{V}_2\text{O}_5$ peak increases in intensity as the 2-propanol concentration crosses a certain threshold for the transformation and $\text{Cu}_x\text{V}_2\text{O}_5$ becomes the dominant phase. The origin of this strong concentration dependence is likely the heterogeneous nature of the reaction, which is expected to be diffusion limited and requires the intercalation of the reducing agent between the CuV_2O_6 layers. The extent of alcohol intercalation within the layered frameworks is expected to depend on the alcohol concentration, since the intimate contact of the reactants can only occur upon the intercalation of the alcohol molecules within the CuV_2O_6 layers.

Notably, the heterogeneous dehydrogenation of alcohols is known to be catalyzed by copper, and indeed forms the basis for a process to synthesize acetone at elevated temperatures (300 °C),^{35–38} conditions not very far removed from those achieved during hydrothermal treatment. Other alcohols (methanol, ethanol, octanol) are analogously able to act as reducing agents as indicated in eq 1, being oxidized to their corresponding aldehydes, ketones, or carboxylic acids in the process.

SEM and TEM images indicate the formation of single-crystalline high-aspect-ratio nanowires of $\text{Cu}_x\text{V}_2\text{O}_5$ upon the hydrothermal reduction of CuV_2O_6 by aliphatic alcohols. The nanowires present a smooth surface and have uniform diameters along the length that are typically <100 nm, as shown in Figure 4. There is no noticeable tapering even in extremely long nanowires. The HRTEM image in Figure 4C illustrates the single-crystalline nature of the nanowires. The lattice spacing of 0.731 nm matches well with the separation between (2 0 0) crystal planes running parallel to the long axis of the nanowire. The single-crystalline nature of these nanowires is in marked contrast to the high concentration of grain boundaries found in CuV_2O_6 nanowires reported previously in the literature.²³ The indexed SAED inset in Figure 4B shows the corresponding planes in the pattern.

The SEM images in Figures 5 and 6 provide further insight into the growth mechanism. Figure 5 shows SEM images of $\text{Cu}_x\text{V}_2\text{O}_5$ nanowires obtained by the hydrothermal reduction

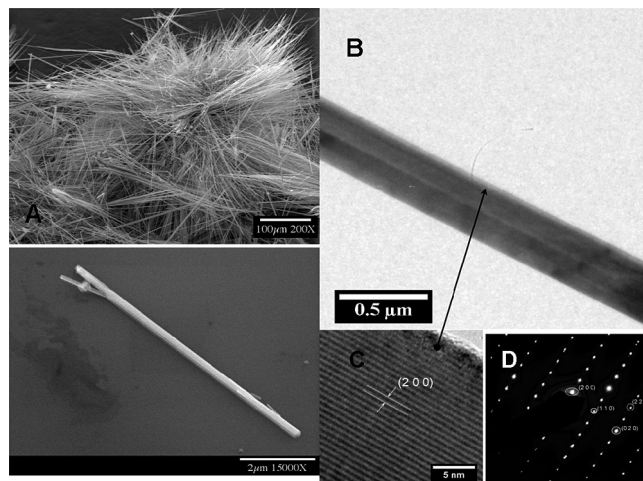


Figure 4. (A) SEM images of $\text{Cu}_x\text{V}_2\text{O}_5$ nanowires showing the high yield of synthesis (top-left), a few single shorter nanowires spin-coated onto a Si/SiO_2 substrate (bottom-left), (B) HRTEM image of two wires, overlapped and aligned, with corresponding (C) showing a lattice-resolved image and (D) indexed SAED pattern of the lattice area.

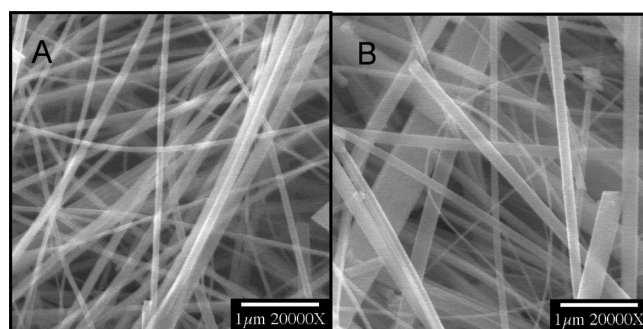


Figure 5. SEM images of $\text{Cu}_x\text{V}_2\text{O}_5$ nanowires prepared by the reduction of CuV_2O_6 by (A) 250 μL 2-propanol, (B) 2 mL octanol.

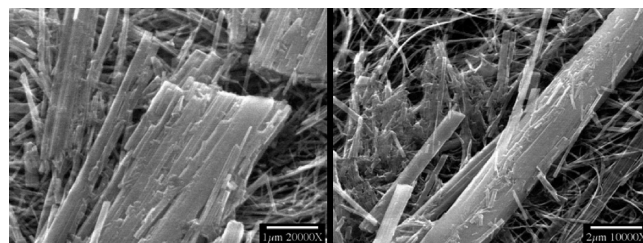


Figure 6. Intermediates observed during the nanowire formation process. The presence of lamellar structures that are splitting into nanowires is clearly evident.

of CuV_2O_6 by different alcohols as per eq (1). Upon reaction for 7 days, methanol, ethanol, 2-propanol, and 1-octanol all yield high-aspect-ratio nanowire geometries, likely being themselves oxidized in the process to aldehydes and ketones or the corresponding carboxylic acids as V^{5+} is reduced to V^{4+} along the V2 ladder and Cu^{2+} is reduced to Cu^+ . We have found no evidence for the formation of volborthite nanowires or the presence of volborthite segments in single-crystalline $\text{Cu}_x\text{V}_2\text{O}_5$ nanowires (vide infra) indicating that the minor phase stays as micrometer-sized particles separable from the nanowires by a gentle centrifugation step. The nuclei of the predominant phase, layered $\text{Cu}_x\text{V}_2\text{O}_5$, are first formed by the disproportionation reaction shown in eq 1. The intercalation/reduction of CuV_2O_6 by the alcohol

(35) Chanda, M.; Mukherjee, A. K. *Ind. Eng. Chem. Res.* **1987**, 26 (12), 2430–2437.

(36) Katona, T.; Molnar, A.; Bartok, M. *Mater. Sci. Eng., A* **1994**, 182, 1095–1098.

(37) Marchi, A. J.; Fierro, J. L. G.; Santamaria, J.; Monzon, A. *Appl. Catal.* **1996**, 142 (2), 375–386.

(38) Molnár, Á.; Varga, M.; Mulas, G.; Mohai, M.; Bertóti, I.; Lovas, A.; Cocco, G. *Mater. Sci. Eng., A* **2001**, 304–306, 1078–1082.

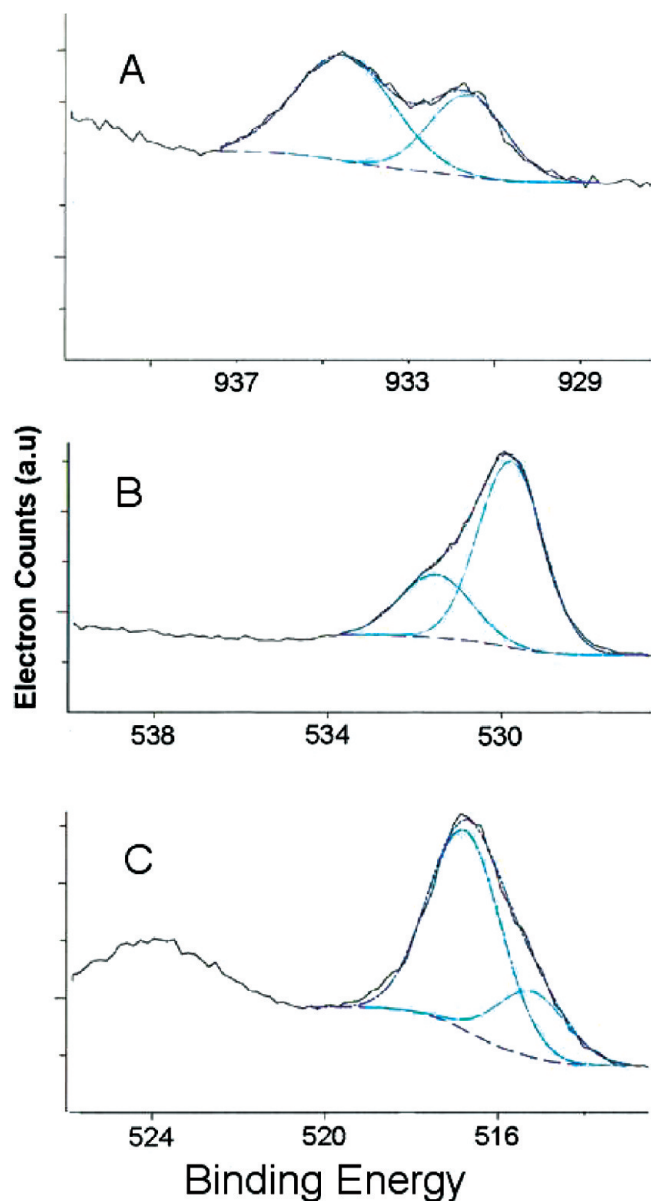


Figure 7. XPS spectra for $\text{Cu}_x\text{V}_2\text{O}_5$ nanowires (A) Copper 2p, (B) Oxygen 1s, (C) Vanadium 2p.

molecules results in the exfoliation of micrometer-sized CuV_2O_6 particles, yielding thin lamellar morphologies. Figure 6 provides clear evidence for the formation of such lamellar intermediates. This figure also shows nanowires being split from the nanosheet intermediates. The splitting of the reduced lamellar intermediates yields $\text{Cu}_x\text{V}_2\text{O}_5$ nanowires as water and alcohol molecules are deintercalated from the layered structure. Similar ripening-exfoliation-splitting mechanisms have been implicated in the formation of 1D nanostructures from other layered precursors. In AgVO_3 , V_2O_5 , and TiO_2 , the stresses generated within exfoliated nanosheets are relieved by disintegration into nanowire fragments. In the reactions reported here, an additional driving force likely comes from the placement of copper in more energetically favorable sites in the β' - $\text{Cu}_x\text{V}_2\text{O}_5$ bronzes.

XPS has been used to further structurally characterize the obtained $\text{Cu}_x\text{V}_2\text{O}_5$ nanowires. Figure 7 shows O 1s, V 2p, and Cu 2p high-resolution XPS spectra acquired for nanowires

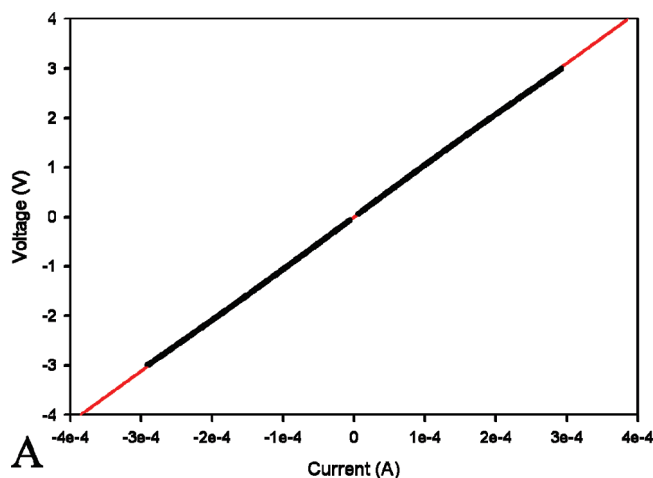


Figure 8. Current vs voltage plot measured for a pressed pellet of $\text{Cu}_x\text{V}_2\text{O}_5$ using the four-point probe technique; least-squares regression fit (red) and data points (black).

ires obtained from the hydrothermal reduction of CuV_2O_6 by 2-propanol for 7 days. XPS data has also been acquired for bulk V_2O_5 and clearly indicates the V^{5+} oxidation state of the orthorhombic framework. For the nanowire samples, the $\text{V}2p_{3/2}$ peak appears at 517.5 eV and the $\text{V}2p_{1/2}$ is at 524.5 eV, yielding a spin-orbit splitting of 7.00 eV.

The O_{1s} region of $\text{Cu}_x\text{V}_2\text{O}_5$ shows multiple peaks evidencing the several crystallographically distinct oxygen sites and different bonding environments in the $\text{Cu}_x\text{V}_2\text{O}_5$ nanowire samples. At least two distinct curves at 529.3 and 531.6 eV can be fitted to the O_{1s} spectra. The $\text{V}2p_{3/2}$ and $\text{V}2p_{1/2}$ region also show broadening, peak multiplicity, and a decrease in the peak energies owing to the reduction of V^{5+} to V^{4+} (and perhaps even some V^{3+}) at 515.3 and 523.8 eV. As noted above, charge disproportionation on the V2 ladder is thought to be the primary origin of the conductivity of these nanowires. The V^{4+} ions observed here likely reside on this V2 ladder and are formed by the reduction of V^{5+} sites in the CuV_2O_6 network during hydrothermal reduction with aliphatic alcohols. Cu^{2+} in CuV_2O_6 is also reduced during the hydrothermal reduction process, and the electrons from the Cu ions occupying interstitial sites may serve to reduce V^{5+} to V^{4+} on the V2 ladder. The $\text{Cu}2p_{3/2}$ region shows distinctive signals corresponding to Cu^{2+} and Cu^+ at 934.6 and 932.4 eV, respectively. Part of the Cu^{2+} signal likely originates from the CuV_2O_6 precursor and volborthite and CuO byproduct noted above. However, it is also possible for Cu^{2+} to occupy some of the interstitial sites within the $\text{Cu}_x\text{V}_2\text{O}_5$ bronzes. Savariault et al. have noted the occupation of tunnel sites by both Cu^+ and Cu^{2+} in micrometer-sized $\text{Cu}_x\text{V}_2\text{O}_5$.³³

Electrical transport measurements support the metallic nature of the synthesized wires. Figure 8 shows the current-voltage plots measured for pellets of $\text{Cu}_x\text{V}_2\text{O}_5$ nanowires by the four-point probe method to eliminate the effects of contact resistance. The linear relationship of the current-voltage curve and the relatively low sheet resistance of 2.7 k Ω suggests the metallic nature of the nanowires (the resistance is <200 times that of a V_2O_5 pellet). Notably, in a pressed pellet measurement, hopping between wires likely

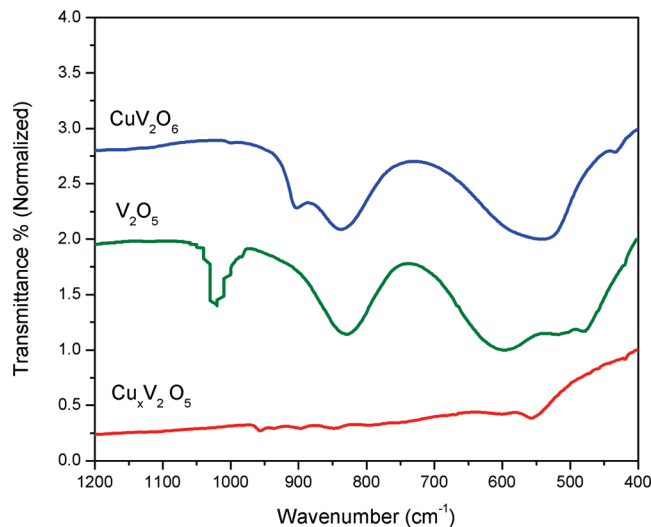


Figure 9. $\text{Cu}_x\text{V}_2\text{O}_5$ (red) infrared absorption is markedly less intense in comparison to the CuV_2O_6 precursor and the empty V_2O_5 framework, evidencing the high carrier density in these nanowires. The plotted spectra have been offset for clarity.

dominates transport but the low resistance values nevertheless evidence the high conductivity of these nanowires.

Fourier transform infrared (FTIR) spectra provide further insight into the electronic structure of the obtained $\text{Cu}_x\text{V}_2\text{O}_5$ bronzes (Figure 9). The V_2O_5 tunnel framework has characteristic IR peaks at 1010, 825, and 500–600 cm^{-1} that can be attributed to V=O stretching (from the vanadyl oxygen), V–O–V coupled stretching, and V–O–V symmetric stretching modes respectively.³⁹ The precursor maintains the absorption characteristics of V_2O_5 at 830 and 550 cm^{-1} but shows a new absorption peak at $\sim 930 \text{ cm}^{-1}$, which is in agreement with Baran and Cabello's study of CuV_2O_6 and the influence of copper in reducing the energy differences between the various V–O bending frequencies.⁴⁰ Remarkably, the IR absorption is very significantly attenuated in the obtained $\text{Cu}_x\text{V}_2\text{O}_5$ nanowires. This is consistent with previous literature results on metallic copper vanadium bronzes and can be attributed to the high carrier concentrations in these metallic nanowires, which strongly suppresses infrared absorption.⁴¹ Very similar IR spectra have been obtained for hydrothermally synthesized nanowires prepared using different aliphatic alcohols corroborating the strong driving force for the stabilization of the $\text{Cu}_x\text{V}_2\text{O}_5$ bronzes upon the reduction of CuV_2O_6 .

Further characterization of the electronic structure of the obtained $\text{Cu}_x\text{V}_2\text{O}_5$ nanowires comes from soft X-ray absorption spectroscopy measurements (Figure 10). NEXAFS is a powerful element-specific tool for probing the frontier orbital states of $\text{Cu}_x\text{V}_2\text{O}_5$ based on the excitation of core hole states to partially filled and empty states. Given the selection rules for NEXAFS, $\Delta l = \pm 1$, the V L-edge NEXAFS spectra represent the d-projected unoccupied density of states,

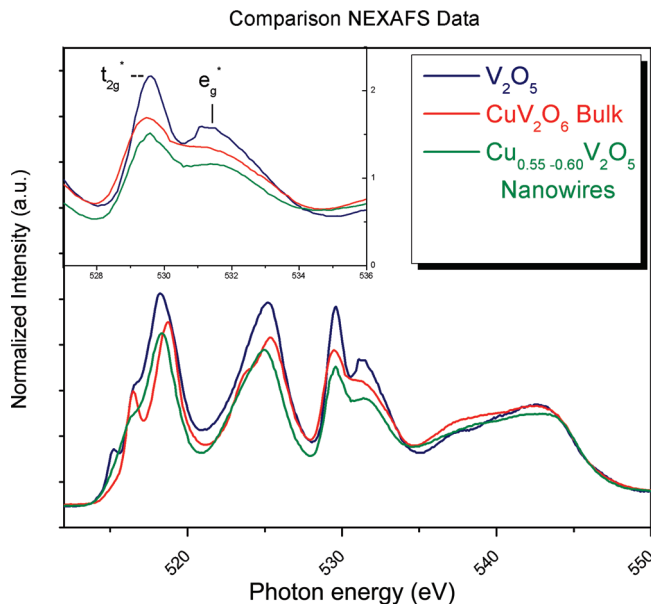


Figure 10. Normalized NEXAFS data for V_2O_5 , CuV_2O_6 , and $\text{Cu}_x\text{V}_2\text{O}_5$ nanowires. The inset shows a magnified view of the O K edge region.

whereas the O K-edge spectra represent the p-projected unoccupied density of states of the valence levels. The strong hybridization of the O 2p levels with the V-3d levels enables the observation of transitions into these unoccupied levels as distinct features in the O K-edge NEXAFS spectra.

The NEXAFS data in Figure 10 shows V L-edge and O K-edge regions for V_2O_5 , the CuV_2O_6 precursor and the β' - $\text{Cu}_x\text{V}_2\text{O}_5$ vanadium bronze nanowires. The two broad peaks centered at ~ 518 and 525 eV are the V L_3 and L_2 peaks arising from $\text{V}2p_{3/2} \rightarrow \text{V}3d$ and $\text{V}2p_{1/2} \rightarrow \text{V}3d$ transitions, respectively. The spin-orbit splitting between the V L_3 and L_2 peaks is 7.0 eV for V_2O_5 , 6.6 eV for CuV_2O_6 , and 6.5 eV for the $\text{Cu}_x\text{V}_2\text{O}_5$ nanowires. Havecker et al. have shown that the positions and lineshapes of V L_3 peaks depend sensitively on both the vanadium formal valence and the local coordination environment as measured by the bond length.⁴² The CuV_2O_6 sample shows a splitting of the V L_3 peak that undoubtedly arises from differences in bond lengths arising from the crystallographically inequivalent V sites in the triclinic crystal structure since the formal valence of all the V sites is V^{5+} in this structure. The V L_3 peak for the $\text{Cu}_x\text{V}_2\text{O}_5$ is more similar to the V_2O_5 data than the spectra for the bulk CuV_2O_6 precursor. Ma et al. have calculated the V 3d projected density of states for the three crystallographically distinct V sites in vanadium bronzes and have shown that differences in the unoccupied density of states for the three types of atoms are very marginal and not enough to explain the observed splitting of the V L_3 peak noted in measurements of bulk vanadium bronze samples.^{15a} A broadening and distinct splitting has also been observed for the vanadium bronze nanowire samples measured here and in analogy to measurements of bulk samples can be attributed to the presence of mixed valence vanadium ions, providing strong evidence for charge disproportionation in these structures.

(39) Mori, K.; Miyamoto, A.; Murakami, Y. *J. Chem. Soc., Faraday Trans.* **1987**, *1* (83), 3303.

(40) Baran, E. J.; Cabello, C. I.; Nord, A. G. *J. Raman Spectrosc.* **1987**, *18* (6), 405–407.

(41) Robb, F. Y.; Glaunsinger, W. S. *J. Solid State Chem.* **1979**, *30* (1), 107–19.

(42) Hävecker, M.; Knop-Gericke, A.; Mayer, R. W.; Fait, M.; Bluhm, H.; Schlögl, R. *J. Electron Spectrosc. Relat. Phenom.* **2002**, *125* (2), 79–87.

Most notably, the difference in the splitting of the L_3 peak (energy difference Δ_1 of 1.95 eV) and the splitting of the O-K-edge peak (energy difference $\Delta_2 = 2.4$ eV) establishes charge disproportionation and not crystallographically inequivalent sites as the origin of the peak multiplicity. Notably, some contribution to the changes in peak position likely arise from the distortion of the VO_6 octahedron to a VO_5 polyhedron and one very weak V–O bond upon the introduction of copper, which causes a small increase in orbital overlap thus raising the energies of the antibonding orbitals. Notably, the low-energy 515 eV peak corresponding to transitions into V $3d_{xy}$ levels hybridized with $2p_x/2p_y$ orbitals on the edge-sharing oxygens in V_2O_5 are lost in the $\text{Cu}_x\text{V}_2\text{O}_5$ nanowires.^{43,44} This split-off conduction band peak is thought to be responsible for the n -type semiconducting nature of V_2O_5 that is no longer retained in $\text{Cu}_x\text{V}_2\text{O}_5$ nanowires.^{43,44} The V L_2 peak is broadened by the Coster–Kronig Auger decay process into a $2p_{3/2}$ hole that does not exist for the L_3 excitation and is less useful for understanding the electronic structure of the nanowires although the splitting of peaks noted above is indeed discernible even for this spectral feature.

The O K-edge spectra of the nanowires can be explained with reference to the data for bulk V_2O_5 . The strong hybridization of O $2p$ states with V $3d$ states leads to the observation of transitions into these orbitals. The splitting of the O K-edge spectra into distinct features arises from the crystal field splitting of the V $3d_{z^2}$ and $3d_{x^2-y^2}$ e_g^* levels from V $3d_{xy}$, $3d_{yz}$, and $3d_{xz}$ t_{2g}^* levels as a result of the roughly cubic field.^{43,44} The intensity of the two peaks relative to the V L-edge resonances arises from the considerable covalency of the V–O bonds, as is typical of early transition metal oxides.⁴⁵ The V_2O_5 experimental data are consistent with previous literature results and spectra predicted from calculated V $3d$ and O $2p$ -projected unoccupied density of states.^{43,44,46,47} The peak at 529.5 represents the O1s transition to $2p_x$ - $3d$ and $2p_y$ - $3d$ overlap orbitals in VO_6 octahedra. The higher energy peak arises from better overlap between $2p_z$ and $3d_{z^2}$ and $3d_{x^2-y^2}$ creating high energy antibonding orbitals for the singly coordinated apical double bond oxygen O(1) in V_2O_5 .^{15a,43} Other contributions to the

O K-edge peaks result from unique two- and three-coordinated oxygen atoms in V_2O_5 . $\text{Cu}_x\text{V}_2\text{O}_5$ is similar to V_2O_5 with clear splitting of the t_{2g}^* and e_g^* peaks. The lineshapes of the O K-edge spectra for $\text{Cu}_x\text{V}_2\text{O}_5$ are remarkably similar which is not surprising given the extent to which the V_2O_5 framework is retained upon the intercalation of copper ions. The peak broadening can be attributed to the presence of a greater number of crystallographically inequivalent oxygens (8 opposed to 3 in V_2O_5). The crystallographically distinct oxygen atoms are expected to be slightly different in the overlapping O $2p$ –V $3d$ hybridization and thus antibonding energies. The levels may also be somewhat hybridized with Cu $3d$ orbitals further modifying the unoccupied density of states in $\text{Cu}_x\text{V}_2\text{O}_5$ nanowires.^{15a} The weakly structured peaks above 535 eV arise from transitions from O1s to O $2p$ levels hybridized with V $4s$ and V $4p$ states. The significant spectral weight in this region further corroborates the strong covalent contributions to bonding in this structure.⁴⁵

In conclusion, single-crystalline copper vanadium bronze nanowires $\text{Cu}_x\text{V}_2\text{O}_5$ have been synthesized via a simple hydrothermal approach based on the reduction of a solid-state CuV_2O_6 precursor by small-molecule aliphatic alcohols. Electron microscopy observations show the formation of clean and uniform wires with aspect ratios exceeding 300. XPS, FTIR, transport, and NEXAFS data evidence charge disproportionation and high carrier densities in the $\text{Cu}_x\text{V}_2\text{O}_5$ nanowires even at room temperature. The availability of these clean nanowire samples will allow investigation of the influence of finite size on the remarkable electronic and electrochemical properties of vanadium bronzes. These high-aspect-ratio copper vanadium bronzes are especially of interest as building blocks for novel cathode architectures showing enhanced Li-ion diffusion kinetics and as highly conducting (and potentially superconducting) elements of nanoscale devices. Future work will focus on transport measurements of individual nanowires to map out the influence of the nanowire dimensions on the quantum phase slips below the critical temperature.

Acknowledgment. S.B. acknowledges startup funding from the University at Buffalo for support of this work. We gratefully acknowledge Dr. Peter Bush and Dr. Yueling Qin for help with SEM and HRTEM measurements. Certain commercial names are presented in this manuscript for purposes of illustration and do not constitute an endorsement by the National Institute of Standards and Technology.

IC802408C

(43) Eyert, V.; Hock, K. H. *Phys. Rev. B* **1998**, *57*, 12727–12737.

(44) Goering, E.; Muller, O.; Klemm, M.; denBoer, M. L.; Horn, S. *Philos. Mag. B* **1997**, *75* (2), 229–236.

(45) de Groot, F. M. F.; Grioni, M.; Fuggle, J. C.; Ghijsen, J.; Sawatzky, G. A.; Petersen, H. *Phys. Rev. B* **1989**, *40* (8), 5715.

(46) Willinger, M.; Pinna, N.; Su, D. S.; Schloegl, R. *Phys. Rev. B* **2004**, *69* (15), 155114/1–155114/7.

(47) Kolczewski, C.; Hermann, K. *Phys. Scr.* **2005**, *T115*, 128–130.